



LAWRENCE
LIVERMORE
NATIONAL
LABORATORY

Electron-Density Scaling of Conversion Efficiency of Laser Energy into L-shell X-rays

K. B. Fournier, C. Constantin, C. A. Back, L. Suter, H.-K. Chung, M. C. Miller, D. H. Froula, G. Gregori, S. H. Glenzer, O. L. Landen

February 2, 2005

Journal of Quantitative Spectroscopy and Radiative Transfer

Disclaimer

This document was prepared as an account of work sponsored by an agency of the United States Government. Neither the United States Government nor the University of California nor any of their employees, makes any warranty, express or implied, or assumes any legal liability or responsibility for the accuracy, completeness, or usefulness of any information, apparatus, product, or process disclosed, or represents that its use would not infringe privately owned rights. Reference herein to any specific commercial product, process, or service by trade name, trademark, manufacturer, or otherwise, does not necessarily constitute or imply its endorsement, recommendation, or favoring by the United States Government or the University of California. The views and opinions of authors expressed herein do not necessarily state or reflect those of the United States Government or the University of California, and shall not be used for advertising or product endorsement purposes.

Electron-density scaling of conversion efficiency of laser energy into L-shell x-rays

K.B. Fournier^{*}, C. Constantin, C.A. Back, L. Suter,
H.-K. Chung, M.C. Miller, D.H. Froula, G. Gregori,
S.H. Glenzer, O.L. Landen

*Lawrence Livermore National Laboratory, 7000 East Avenue, Livermore, CA
94550*

Abstract

Laser-produced plasmas at subcritical densities have proven to be efficient sources for x-ray production. In this context, we obtain new results from experiments performed in Kr and Xe gas-filled targets that were irradiated by the high-power OMEGA (Laboratory for Laser Energetics, University of Rochester) laser. Nearly 40% of the laser energy was converted into x-rays in the L-shell-photon-energy range ($\geq 1.6\text{keV}$) by a Kr-filled target. The conversion efficiency measurements were correlated with time-resolved plasma-temperature measurements done by means of a Thomson-scattering diagnostic. The measured range of temperatures, between 2–3.5 keV, is in good agreement with LASNEX radiation-hydrodynamics simulations. X-ray-cooling rates and charge-state distributions were computed using detailed atomic data from the HULLAC suite of codes. X-ray yields predicted by the cooling-rate calculations are compared to measured spectra, and good agreement is found for predictions made with highly-detailed atomic models. We find that x-ray conversion efficiency in Kr-filled targets is a strong function of temperature, and has an optimum density near 10–15% of the laser’s critical density.

Key words: Laser plasma; X-ray conversion efficiency; Underdense radiator

1 Introduction

An important capability in inertial confinement fusion (ICF) experiments [1] is to diagnose the properties of and the transient phenomena occurring in

^{*} Corresponding author

Email address: fournier2@llnl.gov (K.B. Fournier).

the dense implosion plasmas. To aid in making these types of measurements, the production of bright, multi-keV sources for x-ray scattering [2] and x-ray backlighting has been intensely studied [3–6], with different approaches to the target design [7,8] or to the irradiating drive configuration [9,10]. Recently, the performance of underdense radiators in terms of laser-energy conversion efficiency (CE) into multi-keV x-rays has demonstrated advantages over conventional foil targets [11,12]. The laser energy is coupled to the subcritical plasma by a volumetric heating, which brings the emissivity up to values higher than in the case of a solid disk target by at least an order of magnitude [13]. In the case of the massive, solid targets the energy deposition takes place at the low-density critical surface, and the high-density region of the target that is predominantly responsible for the radiation emission must be heated by a slow thermal-conduction process. In the underdense targets, the laser penetrates more deeply to heat material at lower densities than the critical value; the main mechanism for laser energy absorption is by inverse Bremsstrahlung. A supersonic heating enables a larger volume to produce x-ray emission. The resulting plasma is characterized by a nonlocal thermodynamic equilibrium (non-LTE) regime that is difficult to model accurately with a complete description of the relevant atomic physics. To understand better the radiative properties and predict the x-ray output of underdense targets, current atomic models need to be validated by experimental data acquired over wide ranges of parameters. The plasma parameters reached during the volumetric heating process, as well as the x-ray emission and cooling history of the target are determined by the electron density, n_e , electron temperature, T_e and average ion charge, Z , in the irradiated sample. Therefore, studies of the plasma behavior as a function of these parameters, and accurate determinations of their values, are important in optimizing reliable x-ray sources.

Numerical calculations performed with the LASNEX [14,15] code indicate that greater than 50% of the laser energy can be converted into x-rays for a variety of laser-irradiated gas targets. Figure 1 shows the predicted conversion efficiency for Kr-filled targets emitting at photon energies above 1.6 keV (L-shell of Kr) versus the ratio of the plasma electron density to the critical density, n_{cr} , for 351 nm laser light (open triangles, dashed trace). According to these results, the conversion efficiency increases with the electron density, to 54% at a density of $n_e \approx 0.13n_{cr}$. There are two traces from the simulations in Fig. 1, the lower one is for Kr L-shell output divided by the *total* incident laser energy, the upper trace is for Kr L-shell output divided by only the energy absorbed by the target. The CE drops for the lower-density targets in part because the absorption is going down (46% absorbed at 0.5atm or $0.043n_{cr}$, 68% at 0.75atm or $0.065n_{cr}$). The CE rolls over and begins dropping for densities above $0.13n_{cr}$ (pressure 1.5atm) because the laser-bleaching wave that does the ionization in the gas no longer has a high-enough Mach number to suppress hydrodynamic motion. Consequently, an imploding density wave develops that both stops the laser and increases the parasitic thermal-radiation

losses below 1.5 keV. The increased parasitic losses leave less energy available to heat considerably more mass, and the gas in the target does not get nearly as hot as it does in the lower-pressure simulations. Thus, an optimum condition exists for producing a bright x-ray backlighter. In the following sections we will describe an experiment that measured the CE scaling with electron density in conditions similar to those in the simulations, in targets filled with pure Kr or a mixture of Kr and Xe gases. Our CE measurements are correlated with plasma temperature measurements. For the plasma temperature measurements a desirable diagnostic is one that acts locally, independently of the complications induced by plasma gradients. Therefore we opted for a Thomson scattering measurement [16] that proved to be consistent with the radiation-hydrodynamic calculations using the LASNEX code. We also measured the size and uniformity of the emitting plasma, which are also important aspects of any potential backlighter.

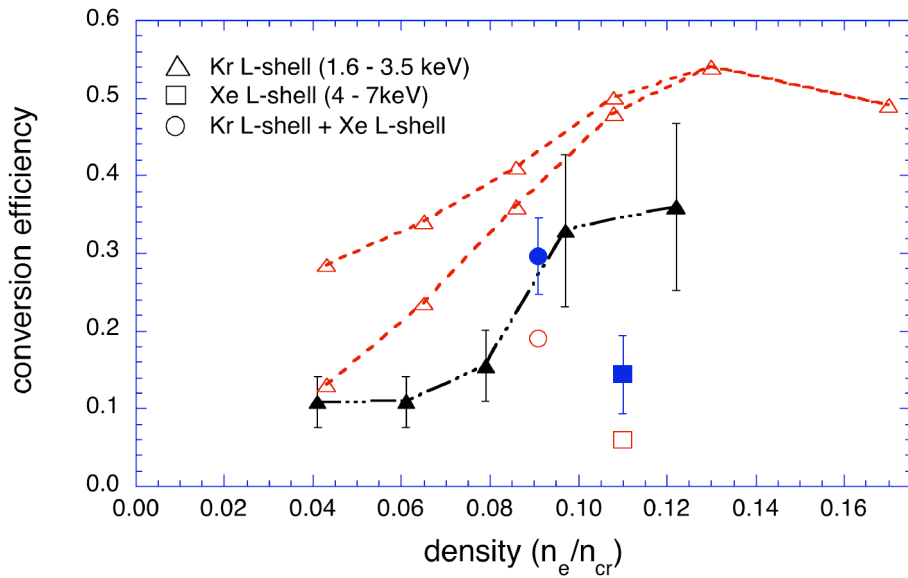


Fig. 1. Predicted (LASNEX) conversion of 3ω laser energy into Kr and Xe L-shell x-ray output as a function of electron density in the target plasma (open symbols). Also shown are the measured results of the present work (filled symbols). The two traces for the Kr L-shell simulations are for x-ray output divided by total incident energy (lower) and by absorbed energy (upper).

We have explained the importance of experimental optimization of x-ray source production and how this work fits in that context. A description of our experimental set-up follows in Section 2. Section 3 reports on the experimental results obtained from the conversion-efficiency, temperature and radiator-size measurements in gas-filled targets. We discuss the numerical simulations of the experiment and the comparison of these calculations (LASNEX and HULLAC codes) with data in Section 4. We conclude and summarize in Section 5.

2 Experimental set-up

The present experiments were performed using 39 beams of the OMEGA laser at $\lambda=351$ nm wavelength (3ω), each of which delivered approximately 500 J in 1 ns pulses, with an average total energy onto the target, $E \leq 19.5$ kJ. The beams were pointed to the target center and defocused by moving the focus 3.5 mm away from the target center, in order to irradiate, homogeneously, as much volume as possible. The resulting individual vacuum beam intensity on target was 2×10^{14} W/cm², with a total of 7.8×10^{15} W/cm² (39 overlapping beams) at the center. The beam overlap region is approximately 800 μm in diameter. Beams are absorbed on their way to the center, also deflection, diffraction and filamentation will affect the intensity at the target center. A second set of measurements was taken with different focusing at a total vacuum laser intensity $I_L=2.3 \times 10^{15}$ W/cm² (overlap region ≈ 940 μm in diameter). The plasmas were formed in irradiated gases confined by polyamide membranes 0.35 μm thick [17,18]. To scale the x-ray conversion efficiency with the electron density, the targets were filled at various pressures between 0.48 atm and 1.47 atm, which correspond to plasma densities between $0.04n_{cr}$ and $0.12n_{cr}$ (where $n_{cr}=9.1 \times 10^{21}$ cm⁻³ for 3ω light). The maximum fill pressure permitted by the thin membrane of the gas enclosure is around 1.5 atm. Pressure transducers attached to the target monitored the gas fill at all times before the laser shot. Thus, the electron densities, which are linearly related to the pressures, are well known for a calculated charge state of the gas (for Kr, $Z=31$, for Xe, $Z=44$) and the neutral gas density. One target contained a mixture of Xe and Kr in equal proportions, at 0.88 atm, which was used to study the influence of a high- Z gas on the laser-x-ray conversion efficiency. For the measurements of the radiator size and uniformity as a function of time a x-ray framing camera with film detection was fielded at 63.4° relative to the target axis. The pinhole-array images were recorded onto four strips separated by ≈ 0.25 ns in time, each with three frames of 60 ps exposure. The x-ray emission of Kr was imaged by filtering the pinholes to allow photon energies ≥ 1.5 keV, while for the Xe-filled targets the filter materials were chosen to cut light below 4 keV.

The x-ray CE was measured using an absolutely flux-calibrated Bragg crystal spectrometer [19], which records time- and space-integrated spectra for energies between 1.5–4 keV, Kr L-shell spectral range, as well as between 4.5–7 keV, Xe L-shell, in the target with the Kr-Xe mixture. The instrument's view of the plasma source was at an angle of 64.4 degrees with respect to the target axis (see Fig. 2). The spectrometer has four channels configured according to the photon energy range to be measured, with a pentaerythritol (PET) crystal for the higher energy channels (Xe L-shell and Kr K-shell) and a rubidium acid phthalate (RAP) crystal for the lower energy channels (for Kr L-shell). The recorded spectra are unfolded by taking into consideration the known crystal reflectivity, transmission through the filters used in front of the spectrometer,

geometry of the crystal mounts and distance to the source (in this set of measurements, about 221 cm). The reflectivity of the crystals and transmission of the filters is known to better than 10% [13]. The CE is defined as the ratio between the total energy in the x-ray emission into 4π divided by the total absorbed laser energy. The x-ray output energy is calculated from the absolute spectra and divided by the incident laser energy, from which the fraction of light scattered due to parametric instabilities [20] is subtracted. In order to evaluate the backscattered signal, we employed a full-aperture backscatter system (FABS), consisting of a system of calorimeters and a streak camera providing time-resolved signals of both SRS and SBS light scattered back into the f/6.7 lens of one of the heater beams that illuminates the target at a 58.79° angle.

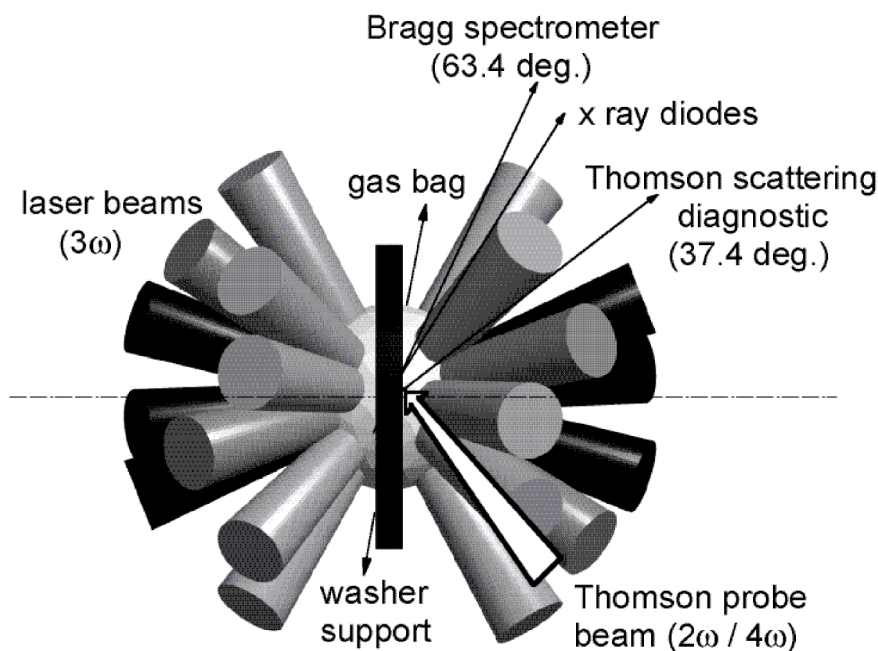


Fig. 2. Experimental set-up with all the laser beams symmetrically irradiating the gas bag target and the main diagnostics shown with their corresponding angles with respect to the target axis.

For plasma temperature measurements a time-resolved Thomson scattering diagnostic was set at 79° with respect to the probe beam (see Fig. 2). The first Thomson scattering experiments with a 2ω ($\lambda=527$ nm) probe beam could only be performed near the edge of the target, before the beam could refract out of the scattering volume. In order to increase the penetration depth of the Thomson probe beam to the target center, a 4ω laser beam ($\lambda=264$ nm) was used in a similar configuration to the 2ω Thomson scattering diagnostic [21]. Scattered light from the plasma was collected by an f/10 lens and coupled to a 1 m spectrometer and a streak camera system with an optical magnification of

1:1. The spectral and temporal resolution of the system, using a 1200 gr/mm grating in the 2nd order were 0.5Å and 50 ps, respectively. The probe beam diameter and entrance slits of the spectrometer and the streak camera defined a cylindrical scattering volume with a 200 μm length and height. The energy of the 4ω probe beam was around 100 J in 1 ns, with a 0.5 ns delay with respect to the heater beams. For our plasma conditions, the scattering parameter is $\alpha=1/(k\lambda_D)\geq 1$ and the scattering is collective (k is the scattering wave vector, and λ_D is the Debye length). The resulting Thomson spectra then show two peaks near the probe laser frequency corresponding to the co- and counter-propagating ion-acoustic waves with the wave number $k=(\frac{4\pi}{\lambda_0})\sin(\theta/2)$, where λ_0 is the fundamental probe-laser wavelength and $\theta=79^\circ$ is the scattering angle. The electron temperature can be directly determined from the separation between the two peaks, which is proportional to $\sqrt{ZT_e}$, if the charge state is known. We have assumed an average charge state of $Z=26-31$ as calculated by radiation-hydrodynamic modeling.

3 Results

The time-integrated spectra obtained from the Kr-filled gas bags at different densities are plotted in Figure 3 over a photon energy range between 1.6–2.6 keV. The emission intensity of all Kr L-shell ions from Kr²⁶⁺ to Kr³³⁺ increases with the electron density, and for all cases the dominant lines in the spectra are the 3G, 3F and 3D Ne-like Kr lines. The weak features at high photon energies are from the B-like to Li-like Kr ions. The quick burn-through from Ne-like to the hotter spectra reflects a broad distribution of charge states attained during the heating and cooling phases of each shot, and emission is integrated over the whole temperature gradient in the target, which is peaked in the central region and drops towards the target edges (see below).

The conversion of the laser energy into Kr L-shell was calculated by summing the time-integrated line emissivities between 1.62–3.5 keV and dividing the x-ray output energy by the laser energy onto the target, from which the fraction of incident light scattered due to stimulated Brillouin and Raman scattering instabilities (SBS and SRS) was subtracted. These fractions were higher for low-density targets, with a maximum value of 5.4% for SBS. All results for the higher-laser intensity are summarized in Table 1 together with the corresponding backscatter levels. The measured CE scales with the electron density, peaking at 0.36 for the highest gas density probed. This is the highest CE value ever reached in an under-dense laser-irradiated target and a very promising result for future bright x-ray sources. The CE measured for the target filled with a mixture of Kr and Xe in equal parts, with an electron density of $0.091n_{cr}$, was calculated by separately accounting for the x-ray output in the Xe and Kr L-shell bands. The Kr L-shell CE=0.186, which, if

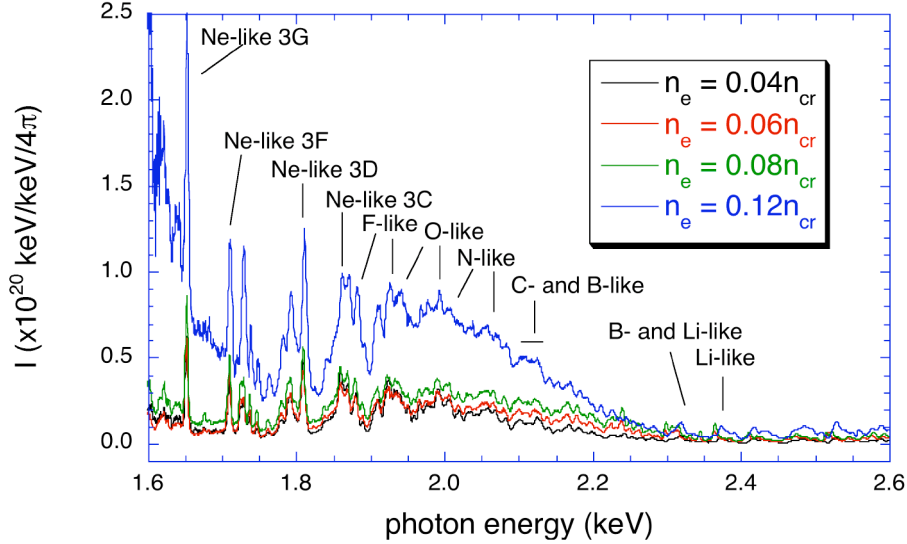


Fig. 3. The measured Kr L-shell spectra for electron densities varying between $0.04n_{cr}$ and $0.12n_{cr}$ (bottom to top). The laser-drive intensity was the same for all experiments.

compared to a pure Kr-target at a density $n_e = 0.097n_{cr}$ that has a CE=0.329, suggests an efficient laser conversion for only half the number of emitters.

Table 1

A summary of the conversion efficiency results in targets containing gases at different pressures. Columns are: the pressure P (atm), the ratio of the electron density to the critical density, the percentages of laser light backscattered through SBS and SRS into the f/6.7 lens, and transmitted through the target, T (measured in only two cases with calorimeters placed after the target), and the conversion efficiency CE for Kr and Xe L-shell.

Gas	P (atm)	n_e/n_{cr}	SBS (%)	SRS (%)	T (%)	CE
Kr	0.48	0.04	5.2	0.	–	0.108
Kr	0.71	0.06	5.4	0.	–	0.110
Kr	0.92	0.08	4.8	0.	–	0.155
Kr	1.14	0.10	3.5	0.	–	0.329
Kr	1.47	0.12	2.0	0.1	0.6	0.360
Kr:Xe	0.88	0.09	2.2	0.04	2.0	0.109 (Xe)
(1:1)						0.186 (Kr)
Xe	0.88	0.11	2.4	0.06	0.7	0.144

The data in Table 1 are also plotted in Fig. 1, along with $\pm 30\%$ error bars, which represent the uncertainty in crystal reflectivity, filter transmission, measured laser energy, scattered energy, and electron density (not more than 20% if the actual average charge Z in the plasma is very different from the as-

sumed $Z=31$). The trends seen in Fig. 1 are worth noting: for the pure Kr targets (triangles), the radiation-hydrodynamics predictions [15] (dividing by *total* incident energy) overestimate the Kr L-shell yields by a factor of two at $n_e \approx 0.06n_{cr}$ and 40-50% at $n_e/n_{cr} > 0.1$, while for the mixed Kr:Xe target (circles), the prediction is 30% too low. A pure Xe target (squares) shot in the higher-laser-intensity configuration gave a L-shell CE of 14.4%, while the LASNEX prediction for that target is too low by 50%. All the data in Table 1 are from the set of experiments with the more tightly focused heater beams, that is, from shots with the higher-laser intensities at the target center. For the lower-intensity case (vacuum $I_L=2.3 \times 10^{15}$ W/cm²), where the peak plasma temperature was measured by the Thomson-scattering diagnostic to be $T_e \approx 3.0-3.5$ keV, a target with the initial electron density of $0.06n_{cr}$ had a CE=0.08 for the L-shell Kr spectrum. This is 30% lower than is measured for the same density target shot in the higher-laser-intensity configuration, where the simulations predict a peak central temperature of 5 keV.

The emission-source size as a function of time has been measured by x-ray imaging. Figure 4 shows targets filled with Kr at $n_e=0.08n_{cr}$ and $n_e=0.12n_{cr}$, and a mixture of Kr and Xe in equal proportions, at $n_e \approx 0.09n_{cr}$. Since the inverse Bremsstrahlung absorption length is given by

$$\lambda_{IB} = \frac{0.56\lambda_L^2 T_e^{3/2}}{(n_e/n_{cr})^2 Z \ln \Lambda} \quad (1)$$

where λ_L is the laser wavelength, Z is the average charge state and $\ln \Lambda$ is the Coulomb logarithm, we expected to observe a clear decrease of the plasma emission length scale with increasing Z and density. The important phenomenon to observe is the rate at which the entire volume that potentially emits in the desired spectral band is filled with radiating plasma for different cases. Therefore, we measured the radial expansion of the plasma emitting during the laser heating with temporal resolution. We observe that for fill pressures of Kr below 1 atm the target is rapidly and entirely filled with the emitting plasma by the time when the laser reaches its peak power. At higher fill pressures, as in the case of the 1.47 atm target (corresponding to a density of $0.12n_{cr}$) the Kr plasma is more collimated on axis, and the edges do not emit in the selected photon energy range (above 1.6 keV). This pattern is similar to what is seen with the emission of the Xe L-shell (photon energies above 4 keV) in the target filled with a Kr-Xe mixture at a pressure below 1 atm. There, the heating process of the gas volume is slower due to the higher Z component in the mixture. Rapid heating and large emission volumes are necessary for imaging with x-ray backlighters, but uniformity across the sample is important, too. After converting the pictures of the 1 atm Kr targets to exposure units using a calibration wedge exposed onto the same piece of film, line outs across the images showed less than 5% variation from the average in exposure at all times while the drive beams were on across a region ≈ 1000

μm in diameter, away from the edges of the bag.

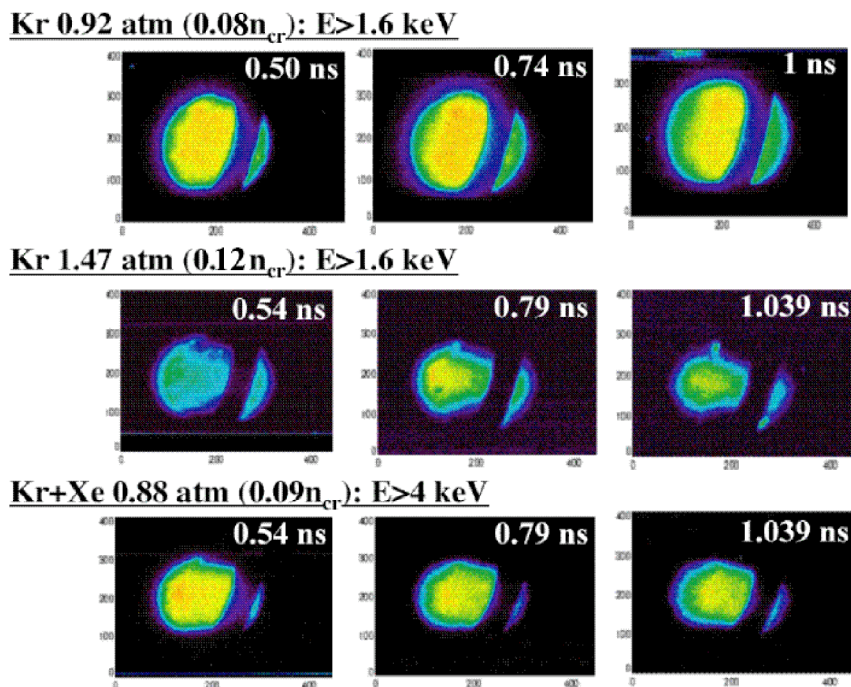


Fig. 4. A selection of x-ray framing camera images at different times during the laser heating of the gas-filled targets. The view is near side-on and observable in the center is the Al washer support ring of the gas bag. The selected targets are Kr-filled gas bags at 0.92 atm and 1.47 atm, followed by a Kr-Xe mixture at 0.88 atm. The laser beams heat the target from both sides. The diagnostic was filtered to image the emission of the Kr above 1.6 keV and the Xe above 4 keV.

Temperature measurements from both the high- and low-laser-intensity shots are shown in Fig. 5 for Kr targets at $0.06n_{cr}$. The target in Fig. 5a is irradiated with a vacuum intensity of $I_L=7.8\times 10^{15}$ W/cm² and in Fig. 5b, $I_L=2.3\times 10^{15}$ W/cm². In case (a) the temperature is inferred from the 2ω Thomson scattering shortly after the end of the laser pulse, which was necessary due to a high background from the plasma self-emission. The scattering volume in this case is located near the target edge, 800 μm away from the center, where the plasma in the given irradiation configuration is cooler. The measured temperature, given by the separation of the ion acoustic features in Fig. 5a is $T_e=1.6$ keV. In the lower laser-intensity case, the plasma was heated with a larger overlap region for the drive beams and smaller gradients are expected, as are lower central temperatures. In these experiments, a 4ω probe beam was used. The scattering geometry for the temperature measurements was similar to the first set of measurements, but the location of the Thomson volume was at the target center. In this measurement the plasma temperature was as high as 3.0–3.5 keV (for $Z=31$ –26, respectively) between $t=0.5$ –0.8 ns, decreasing to 1.8–2.0 keV (for $Z=28.5$ –26, respectively) after the main laser-drive pulse is

turned off (1.25-1.3 ns) [see Fig. 5(b)]. The Thomson-derived temperatures are accurate to $\pm 20\%$ based on the fits to the spectra and the assumed value of Z .

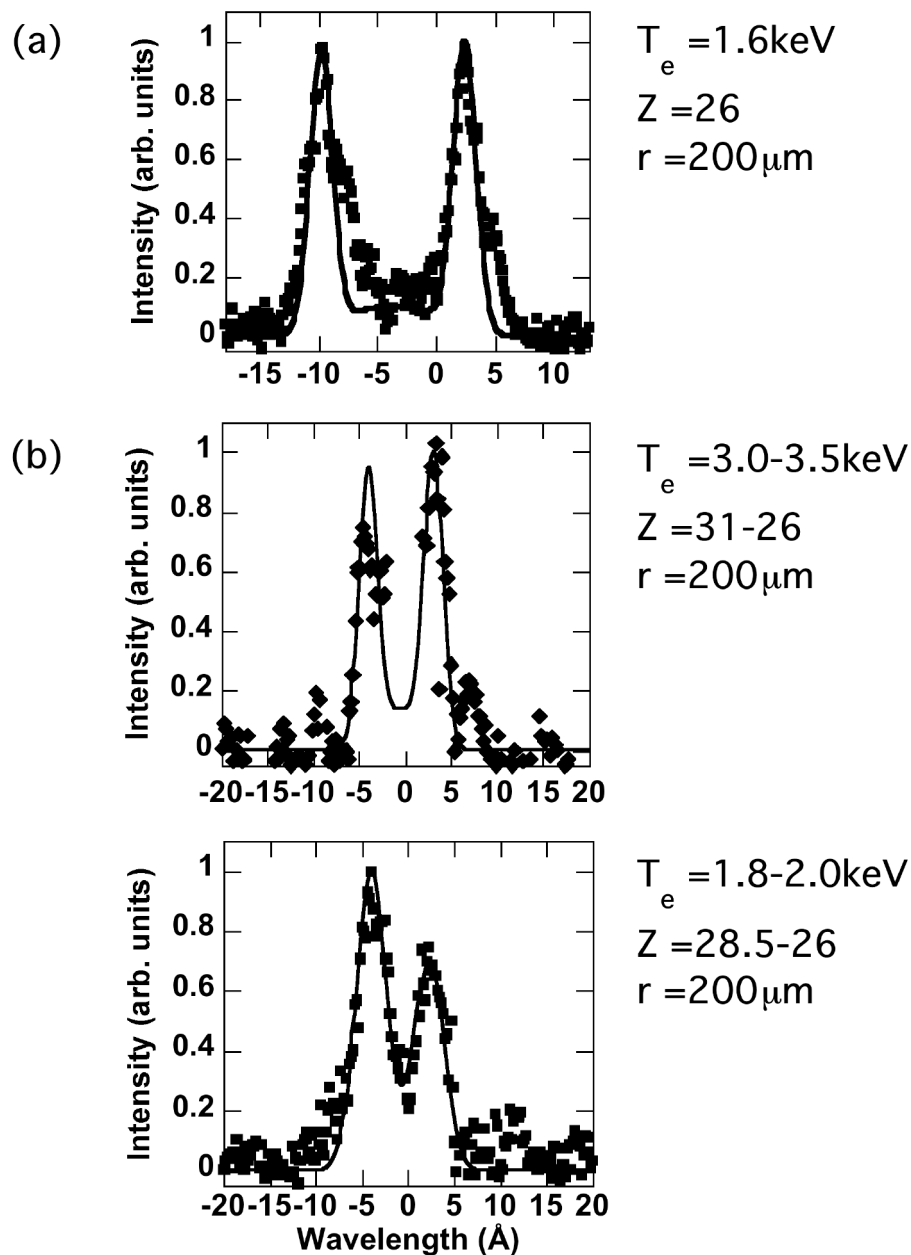


Fig. 5. Measured Thomson scattering spectra for (a) 2ω and (b) 4ω probe beams, along with best fits. The data in (a) are from a volume displaced $800 \mu\text{m}$ from the center of the Kr gas target, at a time after the end of the drive beams. The data in (b) are from the center of the target, at times (top) during the peak laser power, 0.5–0.8 ns and (bottom) after the drive beams have ended, 1.25–1.30 ns. The parameters used in each fit are written next to the spectrum, r is the dimension of the scattering volume.

4 Numerical simulations

To get an insight into the temperature distribution in the Kr plasma, we confronted the measurements performed at different locations in the targets with theoretical models that provide calculated-temperature values. The Thomson scattering measurements indicate a temperature of 1.6 keV at approximately 800 μm from the target center at a time 1.2–1.5 ns after the start of the pulse. In the low-laser-intensity configuration, the core is heated to a temperature of ≈ 3.25 keV during the laser pulse, decreasing in time to ≈ 2 keV after the heater beams turn off. These temperature points were used to benchmark numerical simulations for the two laser configurations. These simulations were performed using the 2D radiation hydrodynamic code LASNEX [14] and the results are in a good agreement with data for both cases, at the Thomson scattering probed locations: (a) 2 keV at 1.2 ns delay from the drive-laser pulse beginning, and (b) 3.42 keV at 0.75 ns delay; 2 keV at 1.5 ns delay. The hot core of the target for the case (a), according to the same calculations, reached a temperature equal to 5 keV during the laser pulse.

We have computed the steady-state collisional-radiative (CR) emissivity of x-ray transitions from all L- and K-shell Kr ions using atomic data from the HULLAC [22] suite of codes. Our models include the fine-structure levels from all singly excited configurations with $n \leq 5$ ($\ell \leq 4$) formed by promotion of an $n=2$ or an $n=1$ electron and some doubly excited configurations formed by permuting the $n=2$ spectator electrons. For some iso-electronic sequences (Mg- to F-like, B- to H-like), levels from configurations with $n \leq 6$ are considered. This results in models with up to > 1600 levels per ion. This significant level of description accounts for only a tiny fraction of the possible dielectronic recombination channels that determine the charge state distribution (CSD) in the Kr plasma. The method used to compute the CSD of the moderate-density plasmas in the present work is described in Ref. [23]. Attention was paid to the collision limit above which levels with principal quantum number n can be neglected; the results in Ref. [23] converge to the earlier coronal result obtained for Kr [24]. The CSDs found for a range of temperatures of interest to the present OMEGA experiments are shown in Fig. 6.

We have computed the steady state CR level populations for all the above-mentioned Kr ions. The atomic structure and rate coefficient data were generated with the relativistic, multi-configuration HULLAC suite of codes. The present models include more than 8000 levels for the sets of ions shown in Fig. 6. Our CR spectrum is compared with data from OMEGA shot 29674 (high-laser-intensity shot, 0.92 atm pressure, $n_e=0.08n_{cr}$) in Fig. 7. Our spectral data are space and time integrated; the observed temperature gradient is reflected in the simulation in Fig. 7 by superposition of spectra from several individual-temperature spectra [25]. The data show emission from all L-shell

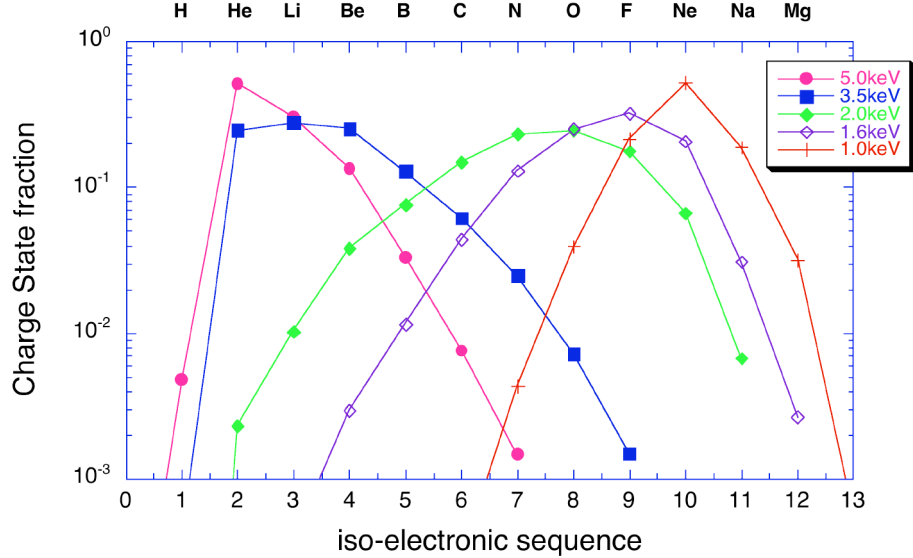


Fig. 6. The calculated CSD for Kr at 1.0, 1.6, 2.0 3.5 and 5.0 keV, computed for $n_e=4.5 \times 10^{20} \text{ cm}^{-3}$. The calculations were done as described in Ref. [23].

ions Kr^{26+} to Kr^{33+} . The data also show a strong recombination phase in the anomalous strength of the 3G and 3F Ne-like lines. This recombination phase is not accounted for in our steady-state calculations. (The HULLAC and LASNEX simulations indicate that the Ne-like Kr lines are optically thin as long as $T_e > 2 \text{ keV}$, thus, the anomalous strength of the 3F and 3G lines is not due to opacity effects.) For the current work, we measure $\approx 3 \text{ kJ}$ of Kr L-shell x-ray output from the spectrum shown in Fig. 7, the theoretical spectrum yields 2.75 kJ in the same spectral band, which is excellent agreement given the crude temperature gradient assumed to weight the steady-state spectra used to construct the simulation in Fig. 7.

5 Conclusions

We have measured the conversion efficiency of 3ω laser light into multi-keV x-rays in the L-shell spectral band of Kr, photon energies between 1.5 and 3.5 keV. The measured CE was steeply increasing with target-plasma density, up to a record 36% at a density $n_e \approx 0.12 n_{cr}$. No saturation of the CE mechanism was observed, due to present limitations imposed by the gas bags' inability to support higher fill pressures. Laser scattering by SBS and SRS instabilities back into the focusing lens became less important as the density increased. In these experiments, we measured the CE of the laser energy to x-rays at two intensities that differed by a factor of three. In the higher-intensity case ($I_L \approx 7.8 \times 10^{15} \text{ W/cm}^2$) steeper temperature gradients across the target are expected due to tighter laser focusing that results in a smaller beam-overlap region. Despite this, the CE into Kr L-shell x-rays is higher in the higher-

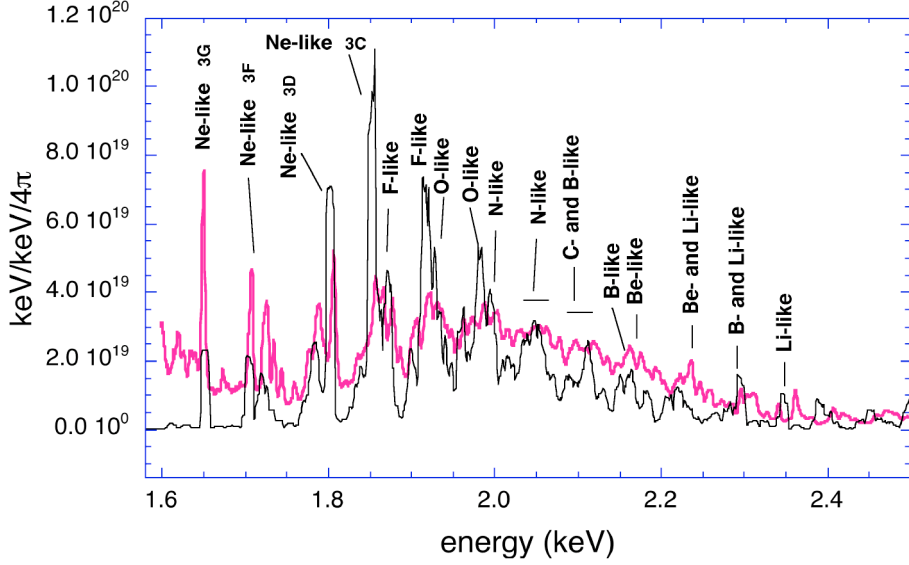


Fig. 7. L-shell Kr spectrum for OMEGA shot 29674 as measured with the HENWAY spectrometer (grey), and a simulated spectrum for a range of temperatures from 1.0 to 4.0 keV using HULLAC atomic data (black). Features from all L-shell ions (Kr^{26+} to Kr^{33+}) are visible.

intensity case. The central temperatures in the low- and high-intensity cases were $\gtrsim 3$ and 5.0 keV, as inferred from Thomson scattering measurements and LASNEX simulations, respectively. The good agreement between the Thomson scattering measurements and the simulated temperatures in the low-intensity case gives confidence in the simulations of the higher-intensity cases (where, in particular, temperature measurements were not performed). On the other hand, the emission in the Kr L-shell band is over predicted by LASNEX, possibly due to the use of an average-atom model [15] that does not calculate sufficient detail for the atomic structure of the Kr L-shell transitions.

A sophisticated atomic model based on HULLAC atomic data was developed for the calculation of Kr L- and K-shell spectra and showed good agreement with the experimentally measured emission, particularly in the higher-photon energy range (B-like Kr^{31+} to L-like Kr^{33+} lines), which is emitted during the peak of the laser-power from the hot core of the target. The calculations indicate that the higher-energy transitions originate in a plasma with $T_e=3.5\text{--}5$ keV, which also agrees with the LASNEX predictions for this region of interest. Spectra calculated for lower-plasma temperatures underestimate the emission in strong Ne-like $2p - 3s$ transitions that is due to enhanced population in these levels following cascades during recombination in the cooling phase of the target; these dynamics are not included in the steady-state spectral simulations. The detailed spectral simulations predict an x-ray yield that is within 10% of what is measured.

For plasma source size, 2D, time-resolved x-ray imaging shows that the largest

emitting volumes are obtained for gas-fill pressures below 1 atm in Kr gasbags. The entire target volume emits radiation above 1.6 keV at 0.5 ns (middle of the laser pulse) and starts to cool slowly after the laser turns off. For large area backlighters, provided the energy range is suitable to a given application, these targets are more appropriate than the higher pressure ones, given that the uniformity can be controlled by tuning the irradiation configuration thus changing the overlap region of the heater beams. For more stringent requirements on brightness, the density in the target has to increase, as our measurements suggest, for the same given input energy. Calculations with LASNEX have shown that to achieve these results (a 40% CE, a large, uniform emitting region) at higher photon energies (4.5 keV in L-shell Xe, 13 keV in K-shell Kr), both gas and underdense solid targets extrapolate very well to the laser powers that will be available at the National Ignition Facility. This work was performed under the auspices of the U.S. Department of Energy by University of California Lawrence Livermore National Laboratory under contract No. W-7405-Eng-48.

References

- [1] Lindl JD, Amendt P, Berger RL, Glendinning SG, Glenzer SH, Haan SW, Kauffman RL, Landen OL, Suter LJ. The physics basis for ignition using indirect-drive targets on the National Ignition Facility. *Phys Plasmas* 2004;11:339-491.
- [2] Glenzer SH, Gregori G, Lee RW, Rogers FJ, Pollaine SW, Landen OL. Demonstration of spectrally resolved x-ray scattering in dense plasmas. *Phys Rev Lett* 2003;90:175002.
- [3] Yaakobi B, Bourke P, Conturie Y, Delettrez J, Forsyth JM, Frankel RD, Goldman LM, McCrory RL, Seka W, Soures JM, Burek AJ, Deslattes RE. High x-ray conversion efficiency with target irradiation by a frequency tripled Nd-glass laser. *Opt Commun* 1981;38:196-200.
- [4] Matthews DL, Campbell EM, Ceglio NM, Hermes G, Kauffman R, Koppel L, Lee R, Manes K, Rupert V, Slivinsky VW, Turner R, Ze F. Characterization of laser-produced plasma x-ray sources for use in x-ray radiography. *J Appl Phys* 1983;54:4260-68.
- [5] Landen OL, Farley DR, Glendinning SG, Logory LM, Bell PM, Koch JA, Lee FD, Bradley DK, Kalantar DH, Back CA, Turner RE. X-ray backlighting for the National Ignition Facility (invited). *Rev Sci Instrum* 2001;72:627-34.
- [6] Workman J, Kyrala GA. X-ray yield scaling studies performed on the OMEGA laser. *Rev Sci Instrum* 2001;72:678-81.
- [7] Turner RE, Amendt P, Landen OL, Glendinning SG, Bell P, Decker C, Hammel BA, Kalantar D, Lee D, Wallace R, Bradley D, Cable M, Craxton RS, Kremens

- R, Seka W, Schnittman J, Thorp K, Murphy TJ, Delamater N, Barnes CW, Hauer A, Magelssen G, Wallace J. Demonstration of time-dependent symmetry control in hohlraums by drive-beam staggering. *Phys Plasmas* 2000;7:333-37.
- [8] Bullock AB, Landen OL, Bradley DK. Relative x-ray backlighter intensity comparison of Ti and Ti/Sc combination foils driven in double-sided and single-sided laser configuration. *Rev Sci Instrum* 2001;72:686-89.
- [9] Phillion DW, Hailey CJ. Brightness and duration of x-ray-line sources irradiated with intense $0.53\mu\text{m}$ laser-light at 60 and 120 ps pulse width. *Phys Rev A* 1986;34:4886-896.
- [10] Kodama R, Mochizuki T, Tanaka KA, Yamanaka C. Enhancement of keV x-ray emission in laser-produced plasmas by a weak prepulse laser. *Appl Phys Lett* 1987;50:720-2.
- [11] Fournier KB, Constantin C, Poco J, Miller MC, Back CA, Suter LJ, Satcher J, Davis J, Grun J. Efficient multi-keV x-ray sources from Ti-doped aerogel targets. *Phys Rev Lett* 2004;92:165005.
- [12] Back CA, Davis J, Grun J, Suter LJ, Landen OL, Hsing WW, Miller MC. Multi-keV x-ray conversion efficiency in laser-produced plasmas. *Phys Plasmas* 2003;10:2047-55.
- [13] Back CA, Grun J, Decker C, Suter LJ, Davis J, Landen OL, Wallace R, Hsing WW, Laming JM, Feldman U, Miller MC, Wuest C. Efficient multi-keV underdense laser-produced plasma radiators. *Phys Rev Lett* 2001;87:275003.
- [14] Zimmerman G, Kruer W. Numerical simulation of laser-initiated fusion. *Comments on Plasma Phys Controlled Fusion* 1975;2:51-61.
- [15] Lokke WA, Grasberger W. XSNQ-U: A Non-LTE Emission and Absorption Coefficient Subroutine. Technical Report, UCRL-52276. Lawrence Livermore National Laboratory, 1977.
- [16] Glenzer SH, Alley WE, Estabrook KG, De Groot JS, Haines MG, Hammer JH, Jadaud JP, MacGowan BJ, Moody JD, Rozmus W, Suter LJ, Weiland TL, Williams EA. Thomson scattering from laser plasmas. *Phys Plasmas* 1999;6:2117-28.
- [17] Kalantar DH, Klem DE, MacGowan BJ, Moody JD, Montgomery DS, Munro DH, Shepard TD, Stone GF, Faylor BH, Hsing WW. Production and characterization of large plasmas from gas bag targets on NOVA. *Phys Plasmas* 1995;2:3161-68.
- [18] Glenzer SH, Fournier KB, Decker C, Hammel BA, Lee RW, Lours L, MacGowan BJ, Osterheld AL. Accuracy of K-shell spectra modeling in high-density plasma. *Phys Rev E* 2000;62:2728-38.
- [19] Koppel LN, Eckels JD. High-resolution x-ray crystal spectrographs. Technical Report, UCRL-79781. Lawrence Livermore National Laboratory, 1977.

- [20] Kruer W. Intense laser plasma interactions - from JANUS to NOVA. *Phys Fluids B* 1991;3:2356-66.
- [21] A. Mackinnon AJ, Shiromizu S, Antonini G, Auerbach J, Haney K, Froula DH, Moody J, Gregori G, Constantin C, Sorce C, Divol L, Griffith RL, Glenzer S, Satariano J, Whitman PK, Locke SN, Miller EL, Huff R, Thorp K, Armstrong W, Bahr R, Seka W, Pien G, Mathers J, Morse S, Loucks S, Stagnitto S. Implementation of a high energy 4ω probe beam on the Omega laser. *Rev Sci Instrum* 2004;75:3906-8.
- [22] Bar-Shalom A, Klapisch M, Oreg J. HULLAC, an integrated computer package for atomic processes in plasmas *J Quant Spectrosc Radiat Transfer* 2001;71:169-88.
- [23] Chung HK, Fournier KB, Lee RW. Non-LTE kinetics modelling of krypton ions: calculations of radiative cooling coefficients. Technical Report, UCRL-JC-149409. Lawrence Livermore National Laboratory, 2002.
- [24] Fournier KB, May MJ, Pacella D, Finkenthal M, Gregory BC, Goldstein WH. Calculation of the radiative cooling coefficient for krypton in a low density plasma. *Nucl Fus* 2000;40:847-64.
- [25] Fournier KB, Back CA, Constantin C, Miller MC, Suter LJ, Chung HK. X-ray emissivities from well characterized underdense, laser-heated gas targets. In: 31st European Physical Society Conference on Plasma Physics, vol. 28G. *Europhysics Conference Abstracts*, 2004. P-5.004.